Inorganic Chemistry

ARTICLE

pubs.acs.org/IC

Light-Driven Transformation of ZnS-Cyclohexylamine Nanocomposite into Zinc Hydroxysulfate: A Photochemical Route to Inorganic Nanosheets

Xiao-Xin Zou,[†,‡] Guo-Dong Li,[‡] Jun Zhao,[‡] Pei-Pei Wang,[‡] Yu-Ning Wang,[†,‡] Li-Jing Zhou,[‡] Juan Su,[†,‡] Lu Li,[†,‡] and Jie-Sheng Chen*[,†]

[†]School of Chemistry and Chemical Engineering, Key Laboratory for Thin Film and Microfabrication of the Ministry of Education, Shanghai Jiao Tong University, Shanghai 200240, P.R. China

[‡]State Key Laboratory of Inorganic Synthesis and Preparative Chemistry, Jilin University, Changchun 130012, P.R. China

Supporting Information

ABSTRACT: ZnS-CHA (CHA = cyclohexylamine) nanocomposite, a unique inorganic−organic hybrid semiconductor, has been prepared from a mild solvothermal reaction system. This material contains 2 nm-sized ZnS nanoparticles, and is photoactive toward UV light (≤300 nm). Under UV-irradiation, the ZnS-CHA nanocomposite is transformed to crystalline zinc hydroxysulfate nanosheets. The driving force of the light-driven transformation reaction is the photogeneration of charges (electrons and holes) in the ZnS nanoparticles, and these photogenerated charges interact with the CHA molecules and the inorganic S^{2-} species, leading to decomposition of the organic component and self-oxidation of the inorganic ZnS nanoparticles to form zinc hydroxysulfate. Through simple thermal treatment, the as-formed zinc hydroxysulfate nanosheets are converted to ultrathin ZnO nanosheets with a porous feature, which exhibit high sensitivity and fast response and recovery for ethanol detection when used as an electrical sensing material.

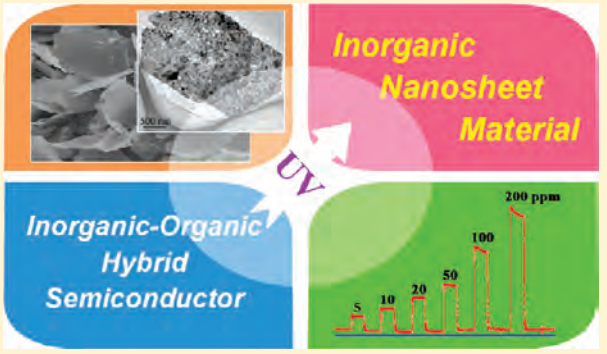

INTRODUCTION

Inorganic nanomaterials often exhibit very attractive properties, and they find applications in a wide spectrum of areas such as optoelectronics, catalysis, biomedicine, and environment protection. Therefore, inorganic nanomaterials have received steadily growing interest in the past decades.[1−4] The ability to generate/manipulate inorganic materials at a nanometer scale is undoubtedly essential to the understanding and further improvement of current nanotechnology. Up to date, many efforts have been devoted to exploring new methodologies in synthesis of inorganic nanomaterials with various structures. Among the existing synthetic strategies, solid-state conversion reactions, by which the obtained products usually inherit the structure/composition features of the solid precursors, are frequently employed to obtain the nanomaterials that cannot be readily acquired using other approaches.[5−13] The most common solid-state conversion route is heat-driven, involving direct thermal transformation from the solid precursor to the desired nanomaterial. For example, many important metal oxide nanostructures have been prepared through calcining metal carbonates,[5−8] metal sulfides,[9,10] or metal alkoxides[11−13] at elevated temperatures.

Recently, we demonstrated that the light-driven solid-state conversion route (LSCR) was highly effective for the preparation of nanoporous TiO_2 material from a titanium-based inorganic−organic hybrid compound.[14,15] The principle of LSCR is very different from that of the heat-driven solid-state conversion route (HSCR). The precursors of LSCR are usually inorganic−organic hybrid semiconductors, and the inherent driving force of LSCR is the photogeneration of charges in the inorganic component of the hybrid semiconductor. The photogenerated charges initiate a series of redox reactions to remove the organic component of the hybrid semiconductor, resulting in the rearrangement of the inorganic species to form a new compound. More importantly, the whole process of LSCR can proceed at room temperature and is rather facile, controllable, and reproducible. The success of LSCR for the formation of nanoporous titania prompted us to explore new inorganic−organic hybrids and to elucidate the effect of light irradiation on its transformation.

In this paper, we report the synthesis of a unique inorganic−organic hybrid ZnS-CHA (CHA = cyclohexylamine) via a mild solvothermal technique. Interestingly, the as-obtained ZnS-CHA nanocomposite is photoactive toward UV light (≤300 nm), and it can be effectively transformed to zinc hydroxysulfate with a sheet-like morphology through UV-irradiation. Furthermore, the zinc

Received: June 14, 2011
Published: August 10, 2011

ACS Publications © 2011 American Chemical Society

hydroxysulfate nanosheets can be thermally converted to ultrathin ZnO nanosheets, which exhibit excellent sensing properties.

EXPERIMENTAL SECTION

Materials. Zinc acetate dihydrate, thiourea, cyclohexylamine (CHA), and ethanol were purchased from Beijing Chemical Factory. The reference ZnO sample was purchased from Tianjin Jinfeng Chemical Industry Co., Ltd. All the reagents were of analytic grade and used as received without further purification. Deionized water was used throughout.

Preparation of ZnS-CHA Nanocomposite. The ZnS-CHA nanocomposite material was prepared through a solvothermal route. In a typical synthesis, zinc acetate dihydrate (0.64 g, 3 mmol) as the zinc source and thiourea (0.45 g, 6 mmol) as the sulfur source were added to CHA (40 mL) and stirred vigorously for 20 min. The mixture was sealed in a 50 mL PTFE-lined stainless steel autoclave and heated at 120 °C for 20 h. After cooling to room temperature, the white ZnS-CHA precipitate was washed several times with ethanol and dried naturally at room temperature. The yield of ZnS-CHA was nearly 100% on the basis of the zinc source used.

Light-Driven Transformation from ZnS-CHA to Zinc Hydroxysulfate. Irradiation of ZnS-CHA under UV-light was performed in a water-cooled quartz cylindrical cell which was illuminated from an internal light source with about 1 cm optical path length. The UV-light source was a 125 W high-pressure mercury lamp, and the irradiation intensity of the UV-light was about 9.1×10^4 μW/cm^2. The ZnS-CHA sample (2.0−3.0 g) was dispersed in water (200 mL) and then exposed to the UV-light irradiation for 7 h. During the irradiation process, gaseous O_2 was bubbled through the solution. After the irradiation, the solid sample was harvested and dried in air. The obtained product was the zinc hydroxysulfate described in the title of this paper, and its yield was about 98% on the basis of the zinc amount.

Formation of ZnO Nanosheets from Zinc Hydroxysulfate. Two ZnO materials were obtained by calcining the zinc hydroxysulfate sample in a muffle furnace at 450 and 750 °C for 2 h, respectively. The corresponding ZnO samples are designated ZnO-450 and ZnO-750, respectively.

General Characterization. The powder X-ray diffraction (XRD) patterns were recorded on a Rigaku D/Max 2550 X-ray diffractometer using Cu Kα radiation (λ = 1.5418 Å). The scanning electron microscopy (SEM) images were taken on a JEOL JSM 6700F electron microscope, whereas the transmission electron microscopy (TEM) and high-resolution TEM (HRTEM) images were obtained on a JEOL JSM-3010 microscope. The FT-IR spectra were acquired on a Bruker IFS 66v/S FTIR spectrometer. The X-ray photoelectron spectroscopy (XPS) was performed on an ESCALAB 250 X-ray photoelectron spectrometer with a monochromated X-ray source (Al Kα $h\nu$ = 1486.6 eV). The energy scale of the spectrometer was calibrated using Au4f$_{7/2}$, Cu2p$_{3/2}$, and Ag3d$_{5/2}$ peak positions. The standard deviation for the binding energy (BE) values was 0.1 eV. The thermogravimetric (TG) analysis for ZnS-CHA was performed in air on a NETZSCH STA 449C TG thermal analyzer from 25 to 800 °C at a heating rate of 10 °C min^{-1}. The UV−vis diffuse reflectance spectra were recorded on a Perkin−Elmer Lambda 20 UV−vis spectrometer. The absorbance spectra were obtained from the reflectance spectra by Kubelka−Munk transformations. The analysis of the organic species present in the UV-irradiation reaction system was performed on a Shimadzu GC-2014C gas chromatograph.

Sensor Fabrication and Testing. The gas sensor was fabricated by pasting viscous slurry of the obtained ZnO sample onto an alumina tube with a diameter of 1 mm and a length of 4 mm, which was positioned with a pair of Au electrodes and four Pt wires on both ends of the tube. A Ni−Cr alloy coil through the tube was employed as a heater to control the operating temperature. Gas sensing tests were performed on a commercial CGS-8 Gas Sensing Measurement System (Beijing Elite Tech Company Limited). For comparison, the sensor performance of the commercially available nanosized ZnO with a particle size of 100−200 nm was also tested.

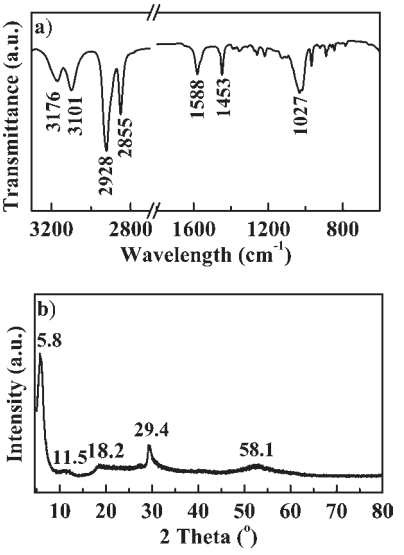

Figure 1. IR spectrum (a) and XRD pattern (b) of the ZnS-CHA nanocomposite.

RESULTS AND DISCUSSION

Preparation and Characterization of ZnS-CHA Nanocomposite. The ZnS-CHA nanocomposite was prepared from a mild solvothermal reaction system, in which cyclohexylamine (CHA) acted not only as the solvent but also as the reactive agent that entered the structure of ZnS-CHA. The presence of CHA in the ZnS-CHA nanocomposite was confirmed by IR spectroscopy (Figure 1a). The characteristic absorption bands associated with CHA appear in the IR spectrum,[16,17] and the stretching vibrations (3176 and 3101 cm^{-1}) and bending vibrations (1588 and 1453 cm^{-1}) of $-NH_2$, the stretching vibrations (2928 and 2855 cm^{-1}) of $-CH_2$, and the stretching vibration C−N (1027 cm^{-1}) are all clearly seen. Figure 1b shows the XRD pattern of the ZnS-CHA nanocomposite. The peaks at 2θ = 29.4 and 51.8° can be assigned to the (002) and (103) planes of wurtzite ZnS. In addition to the two peaks related to ZnS, a strong XRD peak at 2θ = 5.8° and two relatively weak peaks at 2θ = 11.5 and 18.2° are also observed, and these three peaks correspond to the *d*-spacing values of 1.54, 0.77, and 0.47 nm, respectively. The presence of these XRD peaks (2θ < 20°) indicates the formation of mesostructures[18,19] because of the assembly behavior of the CHA molecules.

The TEM measurements further confirm the structure of the ZnS-CHA nanocomposite. The TEM image (Figure 2a) shows a set of black/white spots occurring across the whole ZnS-CHA particle. The HRTEM imaging (Figure 2b) indicates that the black spots are the inorganic ZnS particles with a size of about 2 nm, and the white spots should correspond to the region where the organic component CHA is located. It is noted that the particles of the ZnS-CHA nanocomposite are plate-like with a diameter larger than 1 μm and a thickness larger than 100 nm (see SEM image in Figure 2c). On the basis of the above observations, it is presumed that the ZnS-CHA composite is formed from the very small ZnS nanoparticles through assembly with the CHA molecules.

dx.doi.org/10.1021/ic201289b |*Inorg. Chem.* 2011, 50, 9106–9113

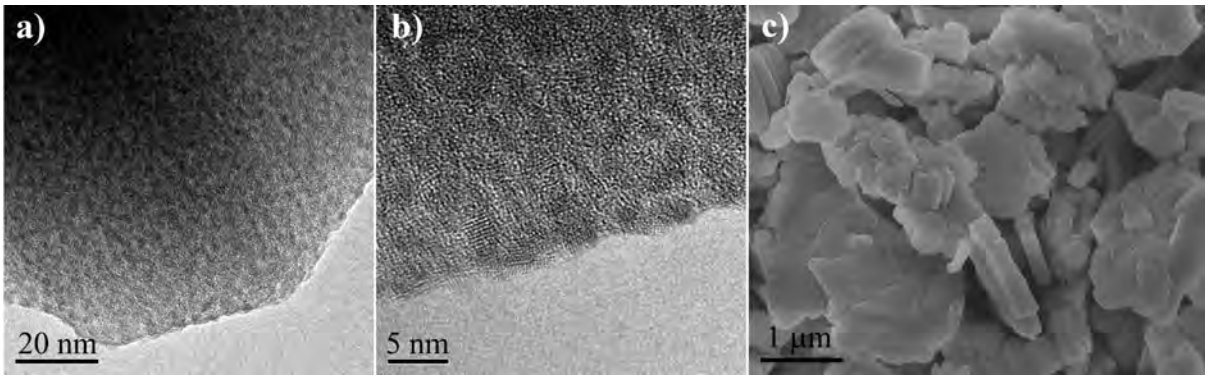

Figure 2. TEM (a), HRTEM (b), and SEM (c) images of the ZnS-CHA nanocomposite.

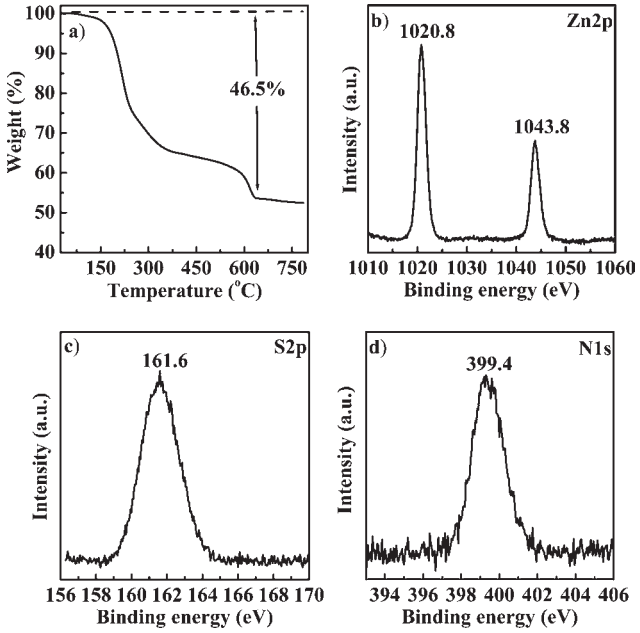

Figure 3. TG curve in air (a), and XPS spectra of (b) Zn2p, (c) S2p, and (d) N1s for the ZnS-CHA nanocomposite.

The thermogravimetric (TG) analysis for ZnS-CHA was carried out in air from 25 to 800 °C, and the corresponding TG curve is shown in Figure 3a. It is seen that the as-synthesized ZnS-CHA material is stable at temperatures below 150 °C, and an obvious weight loss takes place at 150 °C and ends at about 640 °C. A total weight loss of about 46.5% is observed, and this weight loss is attributed to the decomposition of CHA and the oxidation of ZnS nanoparticles to ZnO in the hybrid material. From the weight loss value it is estimated that the empirical composition of the ZnS-CHA nanocomposite is ZnS·0.55CHA. To obtain valuable information about the chemical nature of the elements involved, XPS has been performed for the ZnS-CHA nanocomposite. Figures 3b–d show the XPS spectra of Zn2p, S2p and N1s. The spectrum for Zn2p (Figure 3b) exhibits two peaks at 1020.8 and 1043.8 eV, which are assigned to the $2p_{3/2}$ and $2p_{1/2}$ core levels of Zn^{2+} in ZnS,[20] respectively. The spectrum for S2p (Figures 3c) shows a single peak at 161.6 eV attributable to S^{2-} in ZnS.[20] The spectrum for N1s (Figures 3d) also shows a single peak at 399.4 eV. This binding-energy value is close to that for alkylamine (399.6 eV) but deviated from that of

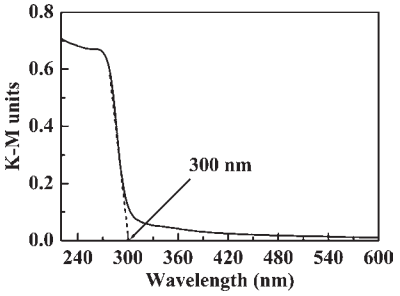

Figure 4. UV–vis diffuse reflectance spectrum of the ZnS-CHA nanocomposite.

alkylammonium (402.4 eV).[17] This observation suggests that the CHA molecules in the ZnS-CHA nanocomposite are not protonated, in agreement with the IR spectrum (Figure 1).

Figure 4 shows the UV–vis diffuse reflectance spectrum of the ZnS-CHA nanocomposite. It is seen that the absorption onset for ZnS-CHA appears at about 300 nm in the ultraviolet region, corresponding to a bandgap energy of 4.13 eV which is larger than that (3.91 eV) of the bulk wurtzite ZnS. The blue shift of absorption onset is attributed to a quantum confinement effect because the size of the ZnS nanoparticles in the ZnS-CHA nanocomposite is smaller than the exciton Bohr radius of ZnS (2.5 nm).[19]

Light-Driven Transformation from ZnS-CHA to Zinc Hydroxysulfate. UV-irradiation of the ZnS-CHA nanocomposite was performed in O_2-saturated water without deliberate addition of any organic/inorganic species. Figure 5 presents the XRD pattern and the IR spectrum of the obtained solid product after the UV-irradiation. It is seen that upon UV-irradiation the XRD diffraction peaks associated with the ZnS-CHA nanocomposite and the IR absorption bands for CHA molecules (Figure 1) completely disappear, and some new diffraction peaks and IR absorptions show up (Figure 5). The new diffraction peaks in Figure 5a correspond to those of zinc hydroxide salts,[6–8,21–23] whereas the IR spectrum (Figure 5b) shows four obvious absorption bands in the region from 500 to 3800 cm^{-1}. A strong and broad IR absorption due to stretching vibrations of OH and a relatively weak absorption due to bending vibration of OH are observed at approximately 3402 and 1647 cm^{-1}, respectively, indicating that a large number of OH groups and water molecules exist in the obtained solid product after UV-irradiation. The two absorption bands at 1119 and 589 cm^{-1} are characteristic of sulfate anions.[24] The X-ray diffraction and the IR spectroscopy indicate that the ZnS-CHA nanocomposite is transformed by UV-

irradiation to zinc hydroxysulfate, accompanied by the removal of the organic components. Indeed, organic species such as ethanol, formaldehyde, and cyclohexylamine have been detected in the aqueous phase through gas chromatography after the UV irradiation of the ZnS-CHA nanocomposite in water. These organic compounds are believed to arise from the decomposition/removal of the organic component in the ZnS-CHA material.

The XPS analysis further confirms the complete conversion of the ZnS-CHA nanocomposite to zinc hydroxysulfate. As shown in the overall XPS spectrum of the zinc hydroxysulfate sample (Supporting Information, Figure S1), only the characteristic peaks of Zn, S, O, and C elements are observed, whereas no XPS peaks of N1s are detected at around 400 eV. This result indicates that no nitrogen is present in the zinc hydroxysulfate and the CHA molecules in the ZnS-CHA nanocomposite are eliminated by UV-irradiation. The weak peak of C1s at around 285 eV is attributed to the signal from adventitious elemental carbon from the XPS instrument.[25] Figures 6b−d present the high-resolution Zn2p, S2p, and O1s spectra of the as-obtained zinc hydroxysulfate. The peaks located at 1021.9 and 1044.9 eV (Figure 6b) are assigned to the $Zn2p_{3/2}$ and $Zn2p_{1/2}$, respectively. In comparison with those in the ZnS-CHA nanocomposite (Figure 3a), the peaks of Zn2p in the zinc hydroxysulfate material show a shift of 1.1 eV toward higher energy, but the distance (23 eV) between the two Zn2p peaks remains unchanged. This phenomenon demonstrates that the zinc species in the ZnS-CHA nanocomposite and zinc hydroxysulfate are both divalent Zn^{2+} cations, but the chemical environments of the zinc cations are different. The single peak located at 170.1 eV (Figure 6b) is attributable to sulfur of SO_4^{2-},[23] and the presence of this peak confirms that under UV irradiation the S species (S^{2-}) in ZnS-CHA nanocomposite are oxidized to SO_4^{2-} in the zinc hydroxysulfate. A quantitative analysis of the XPS data shows that the atomic ratio of Zn/S is approximately 4:1, corresponding to a composition of $Zn_4(OH)_6(SO_4)\cdot nH_2O$ for the obtained zinc hydroxysulfate material. The presence of H_2O and hydroxyl groups (OH) is also supported by the strong XPS peak located at 532.5 eV (Figure 6c).

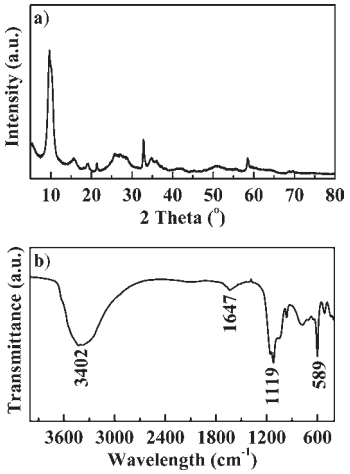

Figure 5. XRD pattern (a) and IR spectrum (b) of the obtained product after UV-irradiation of the ZnS-CHA nanocomposite.

Figures 7a−b show the typical SEM images of the as-obtained zinc hydroxysulfate sample. The images demonstrate that this sample has a sheet-like morphology with a thickness of about 10 nm and a diameter up to several micrometers. The thickness of the zinc hydroxysulfate sample is far smaller than the ZnS-CHA nanocomposite (Figure 2c), demonstrating that the UV-irradiation not only converts the structure of ZnS-CHA at the molecular level, but also varies the morphology of the obtained inorganic product. The TEM image (Figure 7c) further confirms the sheet-like morphology of the zinc hydroxysulfate material. A high-resolution TEM (HRTEM) image taken from the nanosheet edge is displayed in Figure 7d. It is clearly seen that the zinc hydroxysulfate is highly crystalline, and nanocrystals with sizes of 2−3 nm are randomly arranged and tightly interconnected to form the individual nanosheet. Light-driven room-temperature crystallization of inorganic nanomaterials is unusual because in previous reports light-driven synthetic strategy only led to amorphous inorganic products,[14,15] whereas normally the zinc hydroxide salt nanostructures were hydrothermally prepared at temperatures over 90 °C.[6−8]

On the basis of the characterization, a formation mechanism of zinc hydroxysulfate from ZnS-CHA is proposed and briefly described as follows. Upon UV irradiation on ZnS-CHA, electrons are photoexcited from the valence band to the conduction band in the ZnS nanoparticles, leading to the formation of energy-rich electron−hole (e^--h^+) pairs (eq 1).[26] The photogenerated electrons move to the surface of the ZnS, where they are captured by O_2 in water to form oxidative species such as superoxide radicals $O_2^{\bullet-}$ (eq 2). These reactive oxygen species function as an effective oxidizing agent, resulting in the decomposition of CHA molecules in ZnS-CHA. In the meantime, the photogenerated holes located in the valence band directly oxidize and decompose the CHA molecules. The resulting amines in water, which are produced and removed from the ZnS-CHA compound through the UV-irradiation, lead to the formation of OH^- species according to eq 3. On the other hand, the ZnS nanocrystals in ZnS-CHA undergo photocorrosion induced by self-oxidation (eq 4), giving rise to Zn^{2+} and SO_4^{2-} ions. Through reaction of Zn^{2+} with OH^- and SO_4^{2-} ions, the nucleation and growth of $Zn_4(OH)_6(SO_4)\cdot nH_2O$ is realized, as shown in eq 5.

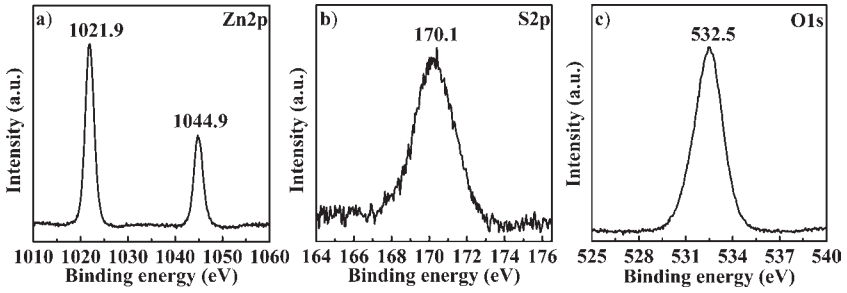

Figure 6. XPS spectra of (a) Zn2p, (b) S2p, and (c) O1s for the solid product after UV-irradiation of the ZnS-CHA nanocomposite.

dx.doi.org/10.1021/ic201289b |*Inorg. Chem.* 2011, 50, 9106–9113

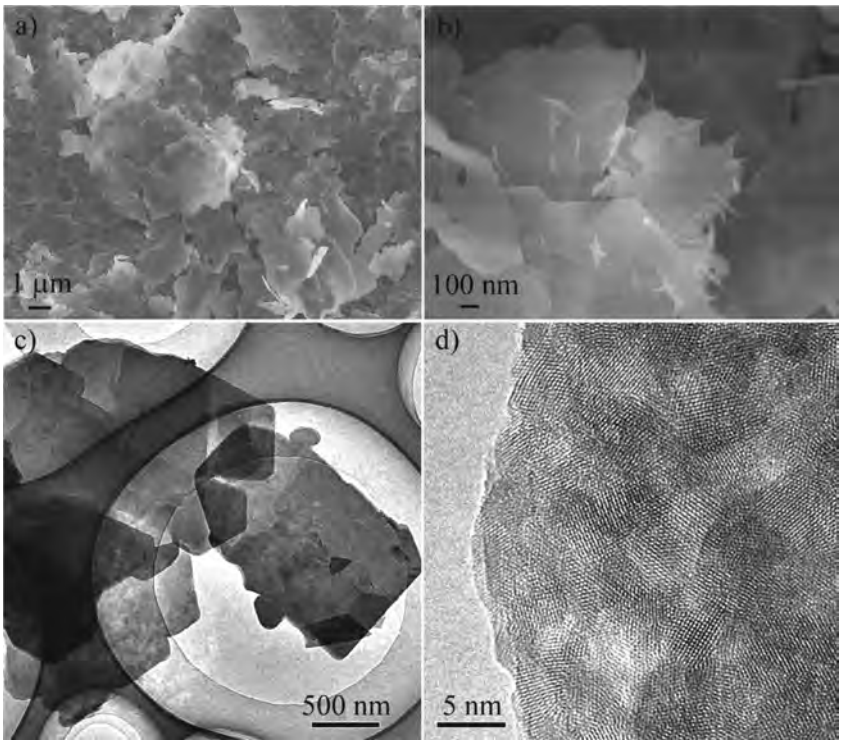

Figure 7. SEM (a–b), TEM (c), and HRTEM (d) images of the zinc hydroxysulfate sample.

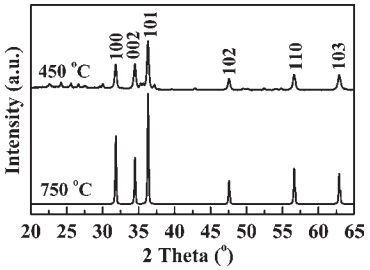

Figure 8. XRD patterns of the ZnO samples obtained by calcining the zinc hydroxysulfate material at 450 and 750 °C.

$$ZnS + h\nu \rightarrow ZnS(e^- + h^+) \quad (1)$$

$$e^- + O_2 \rightarrow O_2^{\cdot -} \quad (2)$$

$$R\text{-}NH_2 + H_2O \leftrightarrow R\text{-}NH_3^+ + OH^- \quad (3)$$

$$ZnS + 4h^+ + 2O_2^{\cdot -} \rightarrow Zn^{2+} + SO_4^{2-} \quad (4)$$

$$4Zn^{2+} + 6OH^- + SO_4^{2-} + nH_2O \rightarrow Zn_4(OH)_6(SO_4)\cdot nH_2O \quad (5)$$

Formation of ZnO Nanosheets. ZnO can be easily formed through calcining the as-synthesized zinc hydroxysulfate at elevated temperatures. Typically, the as-obtained zinc hydroxysulfate was heated at 450 and 750 °C in air, and the resulting ZnO samples are designated ZnO-450 and ZnO-750, respectively. Figure 8 shows that the XRD patterns of the ZnO-450 and ZnO-750 samples. For the ZnO-450 material, a set of strong diffraction peaks ($2\theta > 30°$), which are perfectly indexed to hexagonal wurtzite ZnO, appear in the pattern. Several very weak diffraction peaks ($20° < 2\theta < 35°$) associated with $Zn_3O(SO_4)_2$ are also observed,[21] indicating that the ZnO-450 sample is dominated by the hexagonal wurtzite ZnO with a trace amount of $Zn_3O(SO_4)_2$. Because $Zn_3O(SO_4)_2$ starts to decompose at about 700 °C (eq 6),[27] an attempt was made to eliminate the $Zn_3O(SO_4)_2$ phase by increasing the calcination temperature to 750 °C. As expected, at 750 °C pure ZnO is obtained (Figure 8). On the other hand, it is noted that when the calcination temperature increases from 450 to 750 °C, the diffraction peaks of ZnO are markedly intensified, demonstrating that the particle size of the ZnO crystals increases distinctly with the increase of calcination temperature.

$$Zn_3O(SO_4)_2 \rightarrow 3ZnO + 2SO_2 + O_2 \quad (6)$$

Figures 9a–b show the typical SEM images of the ZnO-450 sample. The images reveal that the material maintains the sheet-like morphology of the zinc hydroxysulfate precursor, with the thickness of the particle being about 10 nm whereas the diameter is larger than 1 μm. A close inspection of the TEM image (Figure 9c) indicates that there exist pores in the ZnO nanosheet, and the HRTEM image (Figure 9d) shows that the ZnO nanosheets are built up from smaller nanocrystals, the size of which is 5–10 nm. The observed lattice spacing is about 0.26 nm, corresponding to the interplanar distance of the (002) reflections for hexagonal ZnO. The SEM images of the ZnO-750 sample are displayed in Supporting Information, Figure S2. It is seen that the particles of this sample maintain the plate-like shape only partly, and the particle thickness (200 nm) of the material is much larger than that of the ZnO-450 sample. The size of the nanocrystals in the individual ZnO plate is over 100 nm.

dx.doi.org/10.1021/ic201289b |*Inorg. Chem.* 2011, 50, 9106–9113

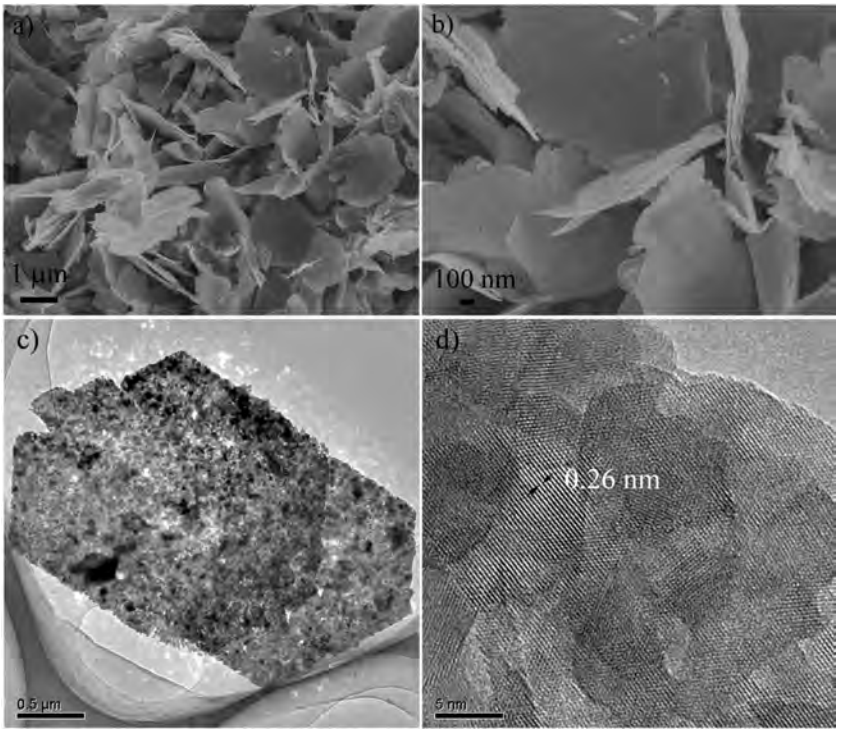

Figure 9. SEM (a–b), TEM (c), and HRTEM (d) images of the ZnO-450 sample.

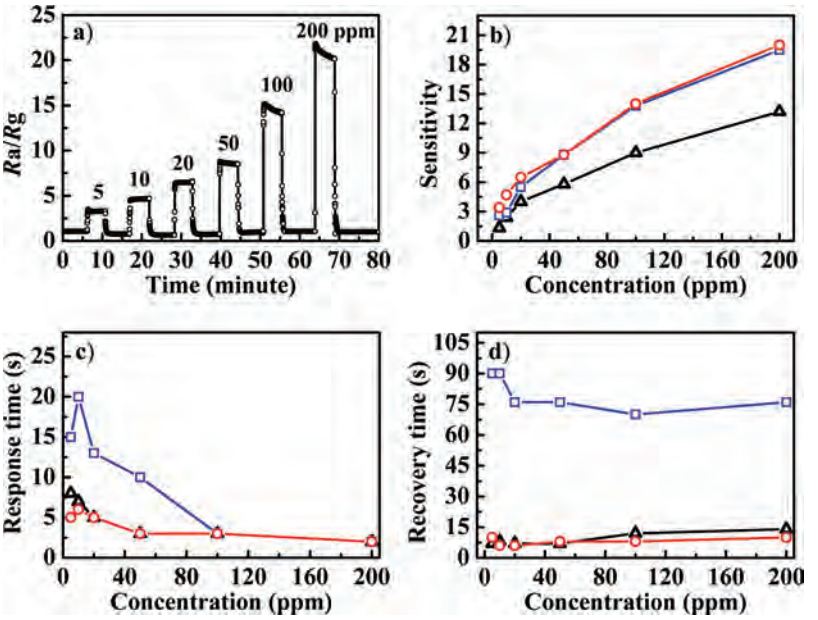

Figure 10. Dynamic response-recovery curve of the sensor based on the ZnO-450 sample with increasing ethanol concentrations (a), and comparison of the gas concentration-dependent sensitivities (b), response time (c), and recovery time (d) of the sensors based on the ZnO-450 (red), the ZnO-750 (blue), and the commercially available ZnO (black) samples.

Sensing Performance of ZnO Nanosheets. The sensing performance of the as-prepared ZnO nanosheets was evaluated using ethanol as the testing gas because ethanol sensors are of importance for breath analysis and food control applications.[6−8,28,29] The optimal operating temperature of the sensor was 280 °C, and the concentration of ethanol varied from 5 to 200 ppm. The sensor sensitivity is defined as the ratio R_a/R_g, where R_a and R_g are the electrical resistance of the sensor in atmospheric air and in the testing gas, respectively. The response and recovery times are defined as the times taken by the sensor to achieve 90% of the total resistance change in the case of adsorption and desorption, respectively.

Figure 10a shows the dynamic response-recovery curve of the sensor based on the ZnO-450 sample with increasing ethanol concentrations. It is seen that the sensor has a wide response

dx.doi.org/10.1021/ic201289b |*Inorg. Chem.* 2011, 50, 9106–9113

range for ethanol from 5 to 200 ppm. When exposed to 5 ppm ethanol, the sensitivity of the sensor is about 3.4. The sensitivity increases significantly with increasing ethanol concentration. For ethanol concentrations of 10, 20, 50, 100, and 200 ppm, the sensitivities are about 4.7, 6.5, 8.8, 14, and 20, respectively. For comparison, the sensor performances of the ZnO-750 sample and the commercially available ZnO material with a particle size of 100−200 nm (Supporting Information, Figure S3) were also tested. Figure 10b shows the gas concentration-dependent sensitivities of the sensors based on the three materials. It is obvious that the sensors based on the as-prepared ZnO-450 and ZnO-750 materials exhibit sensitivities distinctly higher than that based on the commercial ZnO, and the performance of ZnO-450 in terms of sensitivity is superior to that of ZnO-750 at low ethanol concentrations (<20 ppm). More importantly, the ZnO-450 sample we obtained exhibits the best sensing properties among all the ZnO materials containing a sheet-like structure reported so far.[6−8,29] For instance, the maximum sensitivity value described in the literature[7] is 8.79 whereas the corresponding value for the ZnO-450 material is about 14 in the presence of 100 ppm ethanol.

In addition to sensitivity, response and recovery times are also key parameters for a gas sensor.[6−8,28,29] Therefore, the gas concentration-dependent response and recovery times for the sensors based on the ZnO-450, the ZnO-750, and the commercial ZnO samples are also compared. As shown in Figure 10b, the time of response (less than 6 s) and that of recovery (less than 12 s) are comparable for both Zn-450 and the commercial ZnO. Nevertheless, the corresponding times for ZnO-750 are very long, with the response time exceeding 10 s at ethanol concentrations below 20 ppm and the recovery time exceeding 70 s at all ethanol concentrations. From the experimental results it is concluded that the ZnO-450 nanosheets are very promising for the fabrication of ethanol sensors because of their high sensitivity and fast response and recovery.

The excellent sensing performance of the ZnO-450 material is attributed to its ultrathin sheet-like morphology and porous structure. It is known that the sensing mechanism of ZnO is based on resistance variation, which is induced by the interaction between the adsorbed oxygen on the surface of ZnO and the gas molecules to be detected,[6−8,28,29] and the modification of electrical resistance mainly takes place at the grain boundaries.[30,31] The ultrathin sheet morphology and the small ZnO particle size in the nanosheets lead to enhanced number of available reactive sites, and thus improved sensitivity. On the other hand, the presence of the porous feature in ZnO-450 nanosheets provides a high surface-to-volume ratio, facilitating the diffusion of target gases. As a result, the sensitivity of the material is distinctly high, and its response and recovery are fast. It should be pointed out that the unique ZnO-450 material is obtained only through the conversion of the zinc hydroxysulfate with a particular morphology, and to our knowledge, no other synthetic techniques have been successful in achieving similar ZnO products.

CONCLUSIONS

We have demonstrated a unique light-driven strategy for the synthesis of inorganic nanosheet materials using inorganic−organic hybrid semiconductor as the precursor. Differing from that of the heat-driven solid-state conversion, the driving force of the light-driven solid-state conversion is found in the photoexcited charges generated in the inorganic component of the hybrid semiconductor. In particular, the light-driven transformation from ZnS-CHA nanocomposite to zinc hydroxysulfate nanosheets with a crystalline structure is realized at room temperature under UV irradiation. Investigations into this light-driven solid-state conversion reaction reveal that the UV-irradiation not only varies the structure of the inorganic−organic hybrid at the molecular level, but also modifies the morphology of the inorganic nanomaterial. Furthermore, ZnO nanosheets are obtained by simply calcining the zinc hydroxysulfate nanosheets at elevated temperatures, and the ZnO products show superior sensing performance for ethanol detection. Our experimental results provide insights into effects of light-irradiation on solid state transformation of inorganic−organic hybrid compounds, and the strategy reported here is anticipated to open new vistas for preparation of inorganic materials with advanced functions.

ASSOCIATED CONTENT

Supporting Information. Overall XPS spectrum of the zinc hydroxysulfate sample; SEM images of the ZnO-750 and the commercially available ZnO materials. This material is available free of charge via the Internet at http://pubs.acs.org.

AUTHOR INFORMATION

Corresponding Author
*E-mail: chemcj@sjtu.edu.cn.

ACKNOWLEDGMENT

This work was financially supported by the National Basic Research Program of China and the National Natural Science Foundation of China. We thank Xingfu Zhu for the TEM measurement.

REFERENCES

(1) Alivisatos, P.; Barbara, P. F.; Castleman, A. W.; Chang, J.; Dixon, D. A.; Kline, M. L.; McLendon, G. L.; Miller, J. S.; Ratner, M. A.; Rossky, P. J.; Stupp, S. I.; Thompson, M. I. *Adv. Mater.* **1998**, *10*, 1297.
(2) Ozin, G. A. *Adv. Mater.* **1992**, *4*, 612.
(3) Thiaville, A.; Miltat, J. *Science* **1999**, *284*, 1939.
(4) Xia, Y.; Yang, P.; Sun, Y.; Wu, Y.; Mayers, B.; Gates, B.; Yin, Y.; Kim, F.; Yan, H. *Adv. Mater.* **2003**, *15*, 353.
(5) Yu, H.; Wang, D.; Han, M.-Y. *J. Am. Chem. Soc.* **2007**, *129*, 2333.
(6) Zhang, J.; Wang, S.; Xu, M.; Wang, Y.; Zhu, B.; Zhang, S. *Cryst. Growth Des.* **2009**, *9*, 3532.
(7) Li, J.; Fan, H.; Jia, X. *J. Phys. Chem. C* **2010**, *114*, 146845.
(8) Liu, X.; Zhang, J.; Wang, L.; Yang, T.; Guo, X.; Wu, S.; Wang, S. *J. Mater. Chem.* **2011**, *21*, 349.
(9) Liu, J.; Xue, D. *Adv. Mater.* **2008**, *20*, 2622.
(10) Zang, Z.-A.; Yao, H.-B.; Zhou, Y.-X.; Yao, W.-T.; Yu, S.-H. *Chem. Mater.* **2008**, *20*, 4749.
(11) Zou, X.-X.; Li, G.-D.; Guo, M.-Y.; Li, X.-H.; Liu, D.-P.; Su, J.; Chen, J.-S. *Chem.—Eur. J.* **2008**, *14*, 11123.
(12) Wang, Y.; Jiang, X.; Xia, Y. *J. Am. Chem. Soc.* **2003**, *125*, 16176.
(13) Jiang, X.; Wang, Y.; Herricksb, T.; Xia, Y. *J. Mater. Chem.* **2004**, *14*, 695.
(14) Zou, X.-X.; Li, G.-D.; Wang, K.-X.; Li, L.; Su, J.; Chen, J.-S. *Chem. Commun.* **2010**, *46*, 2112.
(15) Zou, X.-X.; Li, G.-D.; Wang, Y.-N.; Zhao, J.; Yan, C.; Guo, M.-Y.; Li, L.; Chen, J.-S. *Chem. Commun.* **2011**, *47*, 1066.
(16) Liu, J.; Guo, Z.; Meng, F.; Luo, T.; Li, M.; Liu, J. *Nanotechnology* **2009**, *20*, 125501.
(17) Gao, Q.; Chen, P.; Zhang, Y.; Tang, Y. *Adv. Mater.* **2008**, *20*, 1837.

(18) Yao, W.-T.; Yu, S.-H.; Wu, Q.-S. *Adv. Funct. Mater.* **2007**, *17*, 623.
(19) Fan, L.; Song, H.; Zhao, H.; Pan, G.; Yu, H.; Bai, X.; Li, S.; Lei, Y.; Dai, Q.; Qin, R.; Wang, T.; Dong, B.; Zheng, Z.; Ren, X. *J. Phys. Chem. B* **2006**, *110*, 12948.
(20) Schwenzer, B.; Pop, L. Z.; Neilson, J. R.; Sbardellati, T. B.; Morse, D. E. *Inorg. Chem.* **2009**, *48*, 1542.
(21) Rojas, R.; Barriga, C.; Ulibarri, A. M.; Malet, P.; Rives, V. *J. Mater. Chem.* **2002**, *12*, 1071.
(22) Newman, S. P.; Jones, W. *J. Solid State Chem.* **1999**, *148*, 26.
(23) Schwenzer, B.; Roth, K. M.; Gomm, J. R.; Murrb, M.; Morse, D. E. *J. Mater. Chem.* **2006**, *16*, 401.
(24) Smith, D. H.; Seshadri, K. S. *Spectrochim. Acta A* **1999**, *55*, 795.
(25) Su, J.; Zou, X.-X.; Li, G.-D.; Wei, X.; Yan, C.; Wang, Y.-N.; Zhao, J.; Zhou, L.-J.; Chen, J.-S. *J. Phys. Chem. C* **2011**, *115*, 8064.
(26) Hoffmann, M. R.; Martin, S. T.; Choi, W.; Bahnemannt, D. W. *Chem. Rev.* **1995**, *95*, 69.
(27) Hongo, T.; Iemura, T.; Yamazaki, A. *J. Ceram. Soc. Jpn.* **2008**, *116*, 192.
(28) Comini, E.; Faglia, G.; Sberveglieri, G.; Pan, Z.; Wang, Z. L. *Appl. Phys. Lett.* **2002**, *81*, 1869.
(29) Jing, Z.; Zhan, J. *Adv. Mater.* **2008**, *20*, 4547.
(30) Feng, P.; Xue, X. Y.; Liu, Y. G.; Wang, T. H. *Appl. Phys. Lett.* **2006**, *89*, 243514.
(31) Wan, Q.; Li, Q. H.; Chen, Y. J.; Wang, T. H.; He, X. L.; Li, J. P.; Lin, C. L. *Appl. Phys. Lett.* **2004**, *84*, 3654.